catalysts

Article

Influence of Power Fluctuation on Ni-Based Electrode Degradation and Hydrogen Evolution Reaction Performance in Alkaline Water Splitting: Probing the Effect of Renewable Energy on Water Electrolysis

Congying Liu [1], Bing Lin [1,*], Hailong Zhang [1], Yingying Wang [2], Hangzhou Wang [3], Junlei Tang [1,3,*] and Caineng Zou [1]

[1] School of Chemical and Chemical Engineering & Institute for Carbon Neutrality, Southwest Petroleum University, Chengdu 610500, China; liucongying135@126.com (C.L.); hailong0902@126.com (H.Z.); zcn@petrochina.com.cn (C.Z.)
[2] Key Laboratory of Optoelectronic Chemical Materials and Devices (Ministry of Education), Jianghan University, Wuhan 430056, China; yingyingwanglyon@126.com
[3] CNPC Shenzhen New Energy Research Institute Co., Ltd., Shenzhen 518000, China; wanghangzhou@petrochina.com.cn
* Correspondence: linbing@swpu.edu.cn (B.L.); tangjunlei@swpu.edu.cn (J.T.)

Highlights:

What are the main findings?

- Square-wave power has the greatest influence on Ni cathode HER compared to step- and triangle-power.
- Increasing the amplitude of square-wave power enhances coated cathode's degradation.

What is the implication of the main finding?

- Guidance for industrializing hydrogen production via renewable energy-coupled electrolytic water.
- Evaluation theory of cathode materials in electrolytic water.

Abstract: The combination of water electrolysis and renewable energy to produce hydrogen is a promising way to solve the climate and energy crisis. However, the fluctuating characteristics of renewable energy not only present a significant challenge to the use of water electrolysis electrodes, but also limit the development of the hydrogen production industry. In this study, the effects of three different types of waveforms (square, step, and triangle, which were used to simulate the power input of renewable energy) on the electrochemical catalysis behavior of Ni plate cathodes for HER was investigated. During the test, the HER performance of the Ni cathode increased at first and then slightly decreased. The fluctuating power led to the degradation of the Ni cathode surface, which enhanced the catalysis effect by increasing the catalytic area and the active sites. However, prolonged operation under power fluctuations could have damaged the morphology of the electrode surface and the substances comprising this surface, potentially resulting in a decline in catalytic efficiency. In addition, the electrochemical catalysis behavior of the prepared FeNiMo-LDH@NiMo/SS cathode when subjected to square-wave potential with different fluctuation amplitudes was also extensively studied. A larger amplitude of fluctuating power led to a change in the overpotential and stability of the LDH electrode, which accelerated the degradation of the cathode. This research provides a technological basis for the coupling of water electrolysis and fluctuating renewable energy and thus offers assistance to the development of the "green hydrogen" industry.

Keywords: fluctuating power; potential shape and amplitude; plate-like HER cathode; water electrolysis

check for updates

Citation: Liu, C.; Lin, B.; Zhang, H.; Wang, Y.; Wang, H.; Tang, J.; Zou, C. Influence of Power Fluctuation on Ni-Based Electrode Degradation and Hydrogen Evolution Reaction Performance in Alkaline Water Splitting: Probing the Effect of Renewable Energy on Water Electrolysis. *Catalysts* **2024**, *14*, 307. https://doi.org/10.3390/catal14050307

Academic Editor: David Sebastián

Received: 30 March 2024
Revised: 23 April 2024
Accepted: 3 May 2024
Published: 6 May 2024

1. Introduction

The warming climate and increasing energy demand constitute the principal contradiction of human society in the present day. It has been projected that by 2050, greenhouse gas emissions will increase by 50%, mainly as a consequence of the expected 70% increase in energy-related CO_2 emissions [1]. To prevent this from occurring, carbon-neutral initiatives intended to reduce greenhouse gas emissions to zero by 2050 are being conducted worldwide [2,3]. Renewable energies, such as solar power, wind power, wave and tidal power, and biomass power, are the most attractive options for decreasing or even eliminating the use of fossil fuels [4,5]. However, the intermittent nature of most renewable energy creates a need for an energy storage method. In this regard, as a carbon-neutral carrier, green hydrogen reduces instability and fluctuation concerns [6,7]. Hydrogen production from renewable resources via electrolysis bears the advantage of complementing the intermittent power supply [8]. Therefore, using renewable energies to forge a hydro-carbon cycle that allows us to create a sustainable green hydrogen-based society is a feasible approach to ensuring our carbon neutrality.

Catalysts are a key factor in the hydrogen production industry's efficiency and economy. Focusing on the reductive side of water splitting, many catalysts for the hydrogen evolution reaction (HER) have been well investigated from various perspectives [9–11]. The purpose of catalyst design is to decrease the reaction energy and improve the reaction kinetics. HER catalysts based on precious metals, such as platinum, are highly robust but suffer from high costs and low abundance [12,13]. Fortunately, nickel, as an abundant non-precious metal on Earth, exhibits excellent corrosion resistance and stability in alkaline electrolytes [14]. Research suggests that nickel ranks just below platinum group metals in hydrogen adsorption of Gibbs free energy, indicating its potential for reversible interconversion of H_2O to hydrogen at low thermodynamic potentials with high efficiency and activity [9,11,15]. Furthermore, nickel has been widely utilized as a HER catalyst in alkaline electrolytic water [16,17].

HER electrocatalysts should meet the following requirements to be practically applied in industry-level production [18,19]: (I) high activity in the HER, (II) strong corrosion resistance in the case of large current fluctuation, (III) great electrochemical stability, (IV) low cost, and (V) timely exchange of reactants and products. The durability and degradation of HER catalytic electrodes have become huge challenges for the hydrogen production industry powered by fluctuating renewable energy. Since the surface of the electrocatalysts must actively adsorb and dissociate from water, their active sites are challenged by the potential for poisoning and destruction during the reactions [18]. Durability/stability testing is usually conducted to observe the corrosion evolution of electrocatalysts [20,21]. Li et al. [22] prepared an amorphous Ni-Fe-Mo-based catalyst for overall water splitting, and the active sites and surface structure of the catalyst improved electron and mass transfer speeds. Furthermore, the electrode showed a high durability at 500 mA cm^{-2} for over 100 h in 1 mol L^{-1} KOH electrolyte. In another study, our research group developed a Ni-based water-splitting self-supported electrode, FeNi-LDH@Ni/SS, with excellent HER and OER performance [23]. The large-scale electrode that we prepared (10 cm × 10 cm) passed 3000 cycles of CV testing and a 100 h 100 mA cm^{-2} stability test, and it showed potential increases of only 18 mV and 21.98 mV, respectively. The stability of HER catalyst electrodes is commonly tested using chronoamperometry (CA) and chronopotentiometry (CP) measurements [18,24–26]. Alternatively, for commercially operating electrocatalysts in the hydrogen production industry, high voltages or current densities are held during production [18]. In addition, new methodologies allowing in situ and precise detection of catalyst dissolution are emerging. These methods provide deep insights into the factors influencing stability and offer novel strategies for ensuring the longevity of electrocatalysts.

However, the majority of research has focused on water electrolysis powered by stable energy, while only a few pieces of research have studied fluctuating power. Wang et al. [27] prepared bifunctional nickel phosphide nanocatalysts for overall water splitting. The cell's capability in terms of water splitting was examined at various current densities from 10

to 100 mA cm^{-2} over 30 h. The authors reported that the catalyst showed outstanding stability and that a change in the structure and composition of the electrode improved water-splitting performance. Kitiphatpiboon and coworkers, meanwhile, synthesized a Ni_3S_2@NiCo-LDH composite electrocatalyst and investigated its durability in an alkaline environment through a multi-current process, which started at 200 mA cm^{-2} and ended at 1000 mA cm^{-2} with an increment of 200 mA cm^{-2} every 500 s before returning to 200 mA cm^{-2} [28]. The authors attributed the steady response of electrochemical reactions to the excellent mass transport, suitable charge transfer properties and high stability of the electrode in a wide range of current densities. Kuroda et al. [29] evaluated catalysts (cobalt nanosheet modified with a tripodal ligand, Co-ns) for alkaline water electrolysis powered by fluctuating renewable energy. According to their durability test, under a cycled potential, Ni catalysts become less useful under fluctuating power, although they present a relatively high performance under a constant current. Alia et al. [30] focused on catalyst degradation with low catalyst loading and intermittent operation for a membrane electrode. The authors simulated the fluctuation conditions of renewable energy by using different wave shapes (hold, triangle wave, square wave), amplitudes, frequencies, and potential ramping (sawtooth, easing square waves). The results indicated that interfacial deterioration of the electrode contributed to durability loss and that higher frequencies and potentials generally resulted in catalytic performance decreasing. In the previous research on the effect of fluctuating power on an electrode, most studies have focused on the degradation of OER electrodes, mainly since a water electrolysis system is strongly affected by sluggish OER progress [29,31,32]. However, power fluctuation also has a huge influence on the HER electrode. In the realm of electro-corrosion science, under stable operation, the HER electrode offers sufficient cathodic protection, while under a fluctuating power supply, incomplete cathodic protection will lead to corrosion of the electrode, which arises from the interaction between electrolyte and electrode degrading the catalytic interface. In addition, the current impact, thermal interaction, and gas–liquid multiphase flow change triggered by the power fluctuation would further result in degradation of the catalytic electrodes and a decrease in HER performance. Against that background, investigating the degradation of HER electrodes contributes to our abilities to couple water electrolysis and renewable energies, and it accelerates the progress that we can make toward realizing carbon neutrality.

In this work, an evaluation method was established for HER electrode degradation and the hydrogen production effect under a condition of fluctuating power. With a view to producing photovoltaic power, the effects of three kinds of power fluctuation shapes on the Ni electrode HER were investigated through electrochemical measurements. Surface analysis methods were employed to understand the degradation behavior of the electrode. Further, we selected the FeNiMo-LDH@NiMo/SS electrode as the cathode, which was prepared via electrodeposition and a hydrothermal method, due to its outstanding catalytic activity for HER and stability in an alkaline environment under stable power supply conditions. This electrode was employed to investigate the effect of power fluctuation amplitude on the electrode degradation and HER effect. In sum, this study was devoted to exploring the hydrogen production behavior of industrial water electrolysis driven by renewable energy, which is of great relevance for the achievement of a sustainable green hydrogen-based society.

2. Results and Discussion

2.1. Effect of Voltage Fluctuation Shape on Electrode Degradation and HER Performance

2.1.1. Time–Current Density Curves of Plate Ni Cathode with Fluctuating Power for HER

In order to investigate the plate Ni cathode's electrochemical behavior when powered by various forms of fluctuating voltage, time (T)–current density (I) curves were recorded, as shown in Figure S1. The current density was positively correlated with the catalytic performance of the Ni cathode. In comparison with the hold voltage results, the current density showed an increase first and then a decrease in behavior during the test with

fluctuating power, which indicated that the surface condition and HER behavior were changed due to the voltage fluctuation. The beginning of test, optimal time and end of test T-I curves are presented in Figure 1a–d, and the average current density (@−1.710 V) at 6 h are given as statistics in Figure 2. The current density was highly responsive to voltage fluctuation, showing the same type of response as that to a change in power input, especially at the beginning of the experiment.

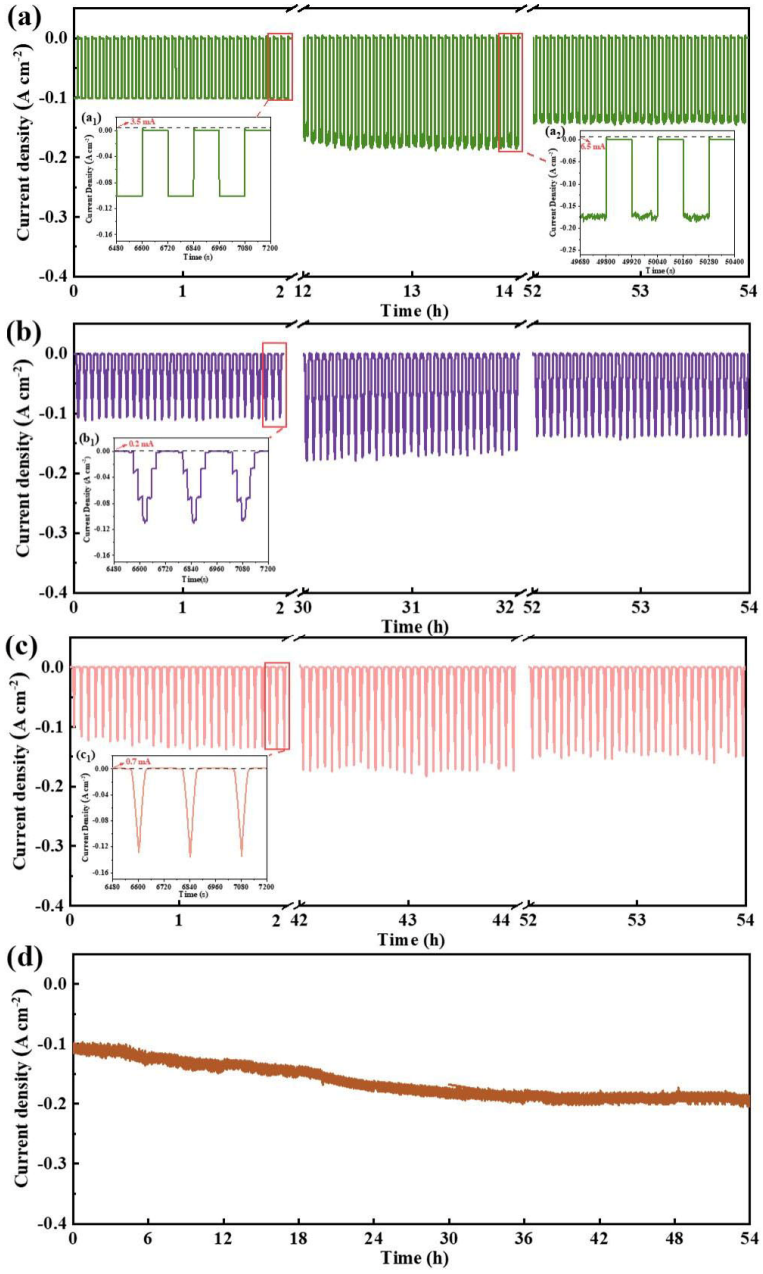

Figure 1. T–I curves of plate Ni cathode in 1.0 mol L^{-1} NaOH solution at 80 °C. (**a**) Powered by square wave voltage. (**b**) Step wave. (**c**) Triangle wave. (**d**) Hold.

For the plate Ni cathode powered by square voltage (Figures 1a and S1a), the T-I curves exhibit an excellent response to the voltage fluctuation in the first 2 h, with the current density reaching 100 mA cm^{-2}@−1.710 V. The current density continues increasing to the maximum current density of about 178 mA cm^{-2}@−1.710 V, with a growth rate of 78% (Figures 1a and 2). The increase in current density indicates the improvement of catalytic activity and hydrogen evolution efficiency [33–35]. In addition, the current density shows a fluctuation range of tens of milliamps at the peak (crest) of the voltage wave as

the test continues, which might be attributed to the changes in the number of active sites and the presence of unstable oxides and hydroxides [36]. The current density gradually declines during the 12 h to the end of the test, and it finally reaches 136 mA cm^{-2}@−1.710 V. The decrease in current density indicates the decrease in HER efficiency of the Ni cathode, which might be attributed to the change in catalytic substance and morphology during square-wave testing. In addition, the fluctuating voltage changes the surface morphology of the catalyst and leads to a change in the electrochemically active surface area [37]. The current density variation trends of Ni cathodes powered by step- and triangle-wave power are similar to that of square voltage. The current density increases at first and then slightly decreases. However, the time at which the maximum current density appears is much later than in the square voltage-powered system, and the maximum current density value is also decreased. For the step wave-powered Ni cathode, the maximum current density appears at 30 h, which is a 74% increase as compared with the initial test. Meanwhile, for the triangle wave test, the maximum current density appears at 42 h and constitutes a 65% increase. The T-I curves reduce in response to voltage fluctuations. When the voltage falls below the onset hydrogen evolution potential (HEP) for the plate Ni cathode (about −1.1 V vs. Hg/HgO (Figure S2)), there is a current density plateau. Although water electrolysis is an endothermic reaction, a higher voltage than the theoretical hydrogen evolution potential is necessary owing to overpotential and ohmic loss [2]. During the voltage increase before reaching the HEP, the cathode current produces a thermal effect according to Joule's law, which leads to double electrode layer change. The square voltage is a transient step to the working potential, the step voltage is a multi-step process, and the triangle voltage is approached as an infinite-step process. Therefore, the thermal work of the response cathode current decreases for each condition, represented as triangle, step, and square voltages. The thermal effect of the current will impact the Ni cathode HER efficiency under a condition of fluctuating power. Greater heat loss leads to less effective energy for hydrogen production, which also affects hydrogen bubbles' behavior and electrodes' durability. The square wave with the largest response current density will have a strong blistering impact, which will influence the cathode surface morphology [36,38]. When the voltage is higher than the HEP, the current used to generate hydrogen will produce the Faradaic process and the ohmic thermal effect. The wave shape may also affect the electrode double layer. For square voltage, the transient change in voltage leads to a hydrogen evolution reaction controlled by the diffusion process of the electrolyte. For step and triangle power, the slower change rate in voltage leads the electrode to react more gently. The fluctuation shape of the voltage can affect the cathode through a thermal effect and mass transport process during water electrolysis, which leads to a change in HER performance and electrode durability. In a control test with a Ni cathode powered by a hold at −1.710 V, the current density slightly increases over the test time. This result strongly indicates that fluctuating power has a significant influence on an electrode's catalytic behavior.

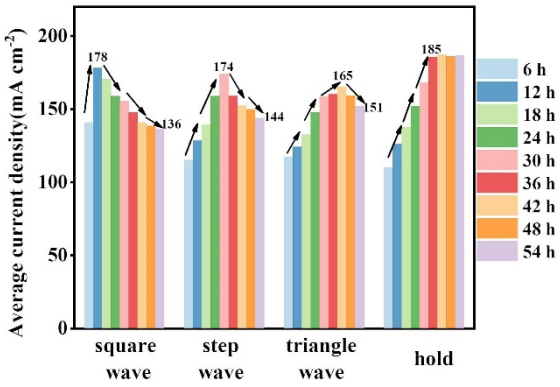

Figure 2. Summarized average peak current density for each 6 h period in the T–I curve of the plate Ni cathode.

It is worth noting that an oxidation current is observed for each square-wave loop instant, dropping from −1.710 V to 0 V. Moreover, the oxidation current density increases from 3.5 mA cm^{-2} for the first 2 h of the test to 6.5 mA cm^{-2} (when the electrode produces the maximum hydrogen production current density). For a Ni cathode powered by step or triangle voltage, the oxidation current density is less than 1 mA cm^{-2}. An oxidation current originates from an electromotive force owing to oxidation reactions [2] during the cathode's return to its original chemical states from a reduced status [39]. The oxidation current is usually associated with a change in electrolytic process, such as on/off operation or a fluctuation in renewable power. The oxidation current leads to the degradation of the cathode due to lower cathode current protection or even anode reactions. Uchino et al. [40] reported a reverse current for a bipolar-type alkaline water electrolyzer, which was believed to be caused by potential changes resulting from redox reactions on the Ni cathode's surface. Haleem et al. [41] reported a harmful current when investigating the relationship between cell stacking position and harmful current generation, as well as changes in potential. They found that rapid changes in potential (during operation start-up) led to electrode degradation. In this study, the oxidation current leads to degradation of the Ni cathode and variation in the cathode current, caused by fluctuating power, which has a synergistic effect on the electrode surface morphology and catalytic efficiency. For the plate-like electrode, the degradation effect enhances surface roughness and increased catalytic active sites. When compared with triangle and step power, square-wave power has the strongest degradation effect, which leads to the earliest timing and largest value of the catalytic current density. After reaching the maximum current density, the persistent destructive effect of fluctuating power would accelerate the degradation of active substances, causing a decline in catalytic performance and durability [2,42,43]. This manifests as current decline in the late stages of tests.

2.1.2. HER Performance Test

To investigate the impact of power fluctuation on the HER performance of the plate Ni cathode, LSV, CV and EIS tests were employed with various shapes of voltages. The original data are shown in Figures S2–S5, and the statistical results are presented in Figure 3.

Figures 3a and S2 reveal a shift in LSV curves and change in overpotential to reach a geometric current density of 10 mA cm^{-2}, with similar trends for various fluctuating powers. For the Ni cathode with square-wave power, the overpotential was 431 mV at the beginning of the test, which significantly dropped in the first 12 h to 347 mV. This result indicated the improved HER activity of the plate electrode with fluctuating power. Then, the overpotential gradually increased to 379 mV, indicating a decline in the HER performance. A similar change process occurred for the Ni cathode with step- and triangle-wave power, for which the minimum overpotentials appeared at 30 h and 42 h, respectively. In addition, we found that the minimum cathode overpotential for square power during the test was the lowest in comparison with those of step and triangle power and that the overpotential of square power at the end of the test was larger than those of the other conditions. This revealed that square-wave power has a greater influence on HER performance in comparison with the other two types of fluctuating powers [30]. In contrast, we also measured the overpotential change for the Ni cathode with a holding voltage, which we found to gradually decline during the test. From this, we surmised that the degradation of the plate Ni electrode was affected by the waveform of the input power voltage, which significantly affected the HER performance in water electrolysis. Next, the ECSA of the Ni cathode with different waveform inputs were measured according to CV curves, and the results are shown in Figures 3b and S3. As can be seen, the ECSAs of the Ni cathode for each condition rapidly rose in the first 12 h. For the fluctuating powered electrodes, the ECSA increases to the maximum value and then changed within a certain range. The ECSA of the electrode powered by the holding voltage, meanwhile, continued increasing throughout the test. As such, the ECSA results corresponded well to the overpotential results. The active sites of HER electrocatalyst on Ni cathode are

associated with the electro-chemical double-layer capacitance (C_{dl}) [44]. Variations in HER performance may be attributed to continuous destruction and reconstruction of the cathode surface with fluctuating voltage. In addition, the destructive effect of fluctuating power is greater for a supported electrode or coated electrode, for which the catalyst is more easily removed, as compared with a self-supported electrode. Accordingly, Tafel slopes and EIS results were generated at the beginning, optimal time, and end of the test to enhance our understanding of the HER behavior of the Ni plate cathode. In addition, the destructive effect of fluctuating power is greater for a supported electrode or coated electrode, for which the catalyst is more easily removed, as compared with a self-supported electrode. Accordingly, the Tafel slope was generated and EIS tests performed at the beginning of the test, optimum time, and the end of the test to further our understanding of the HER behavior of the plate Ni cathode. As shown in Figures 3c and S4, the Tafel slope, calculated using the Tafel equation (η = blogj + a, where b is the Tafel slope), for the beginning of the test was about 150 mV dec-1 for all conditions. Then, the Tafel slope significantly reduced at the optimum time during the test with fluctuating power. The decrease in the Tafel slope indicated fast reaction kinetics [44,45], which mean an improvement in the HER performance and energy utilization efficiency. At the end of the test, the Tafel slope of the Ni cathode slightly increased, which was consistent with the previous results. As the control test, the Tafel slope of the Ni cathode with the holding voltage was generated, which showed a decline and then held steady at about 100 mV dec^{-1}. EIS was performed on the Ni cathode with various voltages, and the Nyquist plots and equivalent circuit are shown in Figure S5. R_{ct} represents the charge transfer resistance during the HER process, and R_1 contributes the surface resistance and delayed detachment of H_2 bubbles [46–48]. Overall, the sum of R_{ct} and R_1 reflects the surface state of the Ni cathode (Figure 3d). Under varying fluctuating voltages, the obtained R_{ct} + R_1 value first decreased and then increased during the test time. This result indicated that the fluctuating electricity increased the electronic transfer rate of the HER electrode.

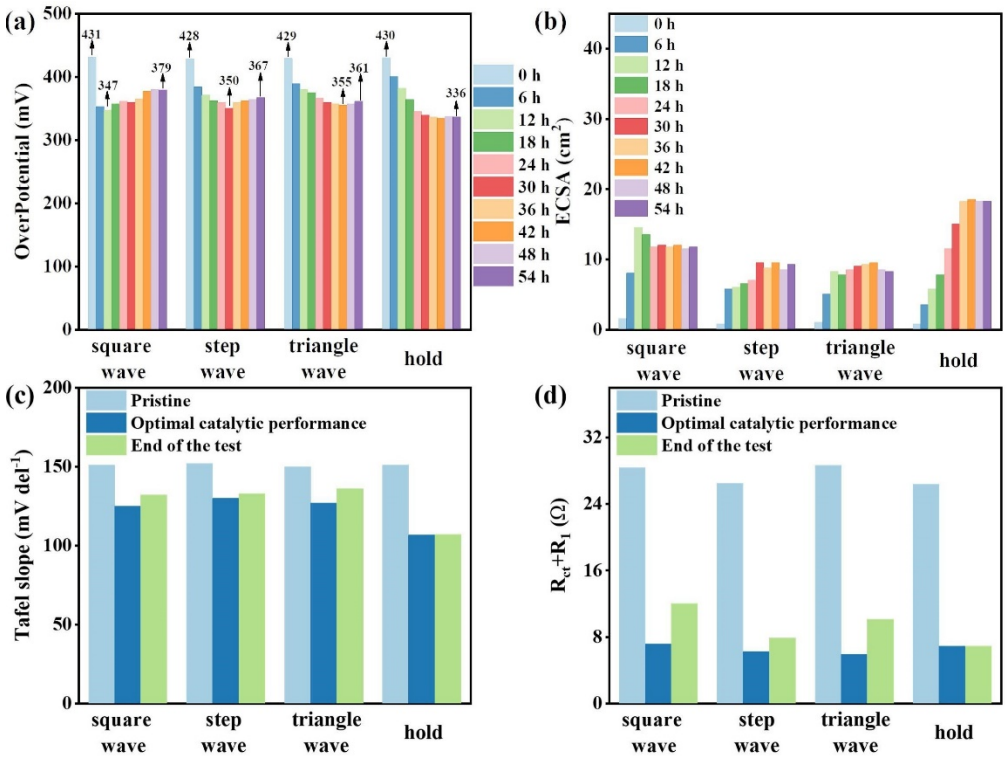

Figure 3. (**a**) Overpotential at 10 mA cm^{-2}, (**b**) ECSA, (**c**) Tafel slopes, (**d**) R_{ct} + R_1 for palte Ni cathode powered by various shapes of voltage and for different times.

In summary, the fluctuating power waveform significantly influenced the HER performance of the plate Ni cathode, and the square voltage showed the maximum effect for the electrode. The optimum HER performance of the square voltage-powered Ni cathode appeared at 12 h with a decrease in overpotential, Tafel slope, and reaction resistance, and the input power affected the HER process in both thermodynamics and dynamics. The oxidation current was an important reason for the surface condition change in the electrode with fluctuating power, which led to a redox reaction of the catalyst. The fluctuating power also led to the destruction and reconstruction of the electrode surface. In contrast, the electrode with the holding voltage showed a continuous change during the test, which further proved the effect of the fluctuating power challenge on an electrode's durability and stability.

2.1.3. Surface Characterization of Plate Ni Cathode with Fluctuating Power

Surface analysis measurements via SEM, AFM and XPS were taken of the Ni cathode with different types of fluctuating power at the beginning of the test, with the maximum current, and at the end of the test. As a control test, surface characterizations of the Ni cathode with the holding voltage were also performed.

The surface morphology of the Ni cathode is presented in Figure 4 (for square-wave and holding-voltage power) and Figure S6 (for step- and triangle-wave power). For the pristine Ni cathode, the smooth surface without blemishes indicated a decent surface condition, as confirmed by the SEM and AFM results. After the HER test was conducted for a certain duration with various fluctuating powers, the Ni cathode showed obvious scratching, defects, lamellar covering, and a porous structure, which were possibly attributable to the transient voltage variations [49,50]. For the cathode reaction in an alkaline electrolyte, first comes the Volmer step:

$$H_2O + e^- + {}^* \leftrightarrow H^* + OH^- \quad (1)$$

and then the Heyrovsky step proceeds:

$$H^* + H_2O + e^- \leftrightarrow H_2 + OH^- + {}^* \quad (2)$$

where * represents the active catalytic site.

During cathodic catalysis, large amounts of OH^- stimulate the production of nickel hydroxide [51]. According to the Pourbaix diagram for Ni/H_2O [20], for water reduction potential in a strong alkaline environment, a Ni cathode would be the Ni or Ni hydroxide [20,52]. With fluctuating power, the cathode state cannot be sustained in the water reduction potential, and a higher potential would lead to the oxidation of Ni and Ni hydroxide to form NiOOH or Ni oxides. The roles of NiOOH and Ni oxides in HER catalysis are inferior to those of Ni and Ni hydroxide [53]. The formation of Ni oxides leads to a decline in catalytic active sites, which results in a decrease in HER performance for the Ni cathode with fluctuating power. These rapidly generated Ni oxides and hydroxides with weak adhesion force to the cathode significantly increase the surface roughness of the cathode. An increase in surface area increases the electrochemically active surface area. Thus, the contradictive effect on HER performance brought about by fluctuating power in our study led to HER variation in the plate Ni cathode. In the T-I curves, the HER performance increased at first, mainly due to the increased active surface area. As the fluctuation test continued, the effect of the reduction in active sites gradually came to dominate, and the HER effect slightly declined. In addition, the oxidation current observed in the T-I curves indicated oxidation reactions on the cathode during the voltage drop, which led to the dissolution of elemental Ni [42,54,55]. The continuously changing voltage promoted the adsorption of high-valence Ni. The dissolution of Ni had similar effects on the catalytic active sites and surface roughness.

XPS was performed on the Ni cathode for each condition to further our understanding of the surface composition. As shown in Figure S7, for the pristine Ni cathode, the characteristic peaks of Ni, NiO, $Ni(OH)_2$ and Ni_2O_3 could be found on the high-resolution

Ni 2p spectrum [51,56,57]. The relative percentages and surface roughness according to AFM of the surface Ni species are summarized in Figure 5. For the square wave-powered condition, the $Ni(OH)_2$ content was over 80%, and the root mean square roughness (R_q) for the optimum HER performance was about 69 nm. As the HER time increased, the $Ni(OH)_2$ content showed little difference, while R_q significantly increased to 137 nm. For the Ni cathode with step or triangle power, similar variations could be observed. Thus, it can be inferred that the square-wave power has larger influence on surface morphology and oxidation conditions. With respect to the cathode with the holding voltage, Ni^0 could be found on the cathode surface, and the change in roughness was moderate. For the cathode-performed HER test with fluctuation power, the peaks of Ni and NiO disappeared, which indicating the oxidation state was enhanced. Specifically, $Ni(OH)_2$ content was dominant on the cathode surface. This result indicated the fluctuating power induced the conversion of the Ni surface to $Ni(OH)_2$ [53]. Combining the AFM results, it became clear that the R_q of the Ni cathode after the HER test was also increased. A catalysis system is dominated by active sites, and the active reaction area is formed under fluctuating power for the plate-like electrode.

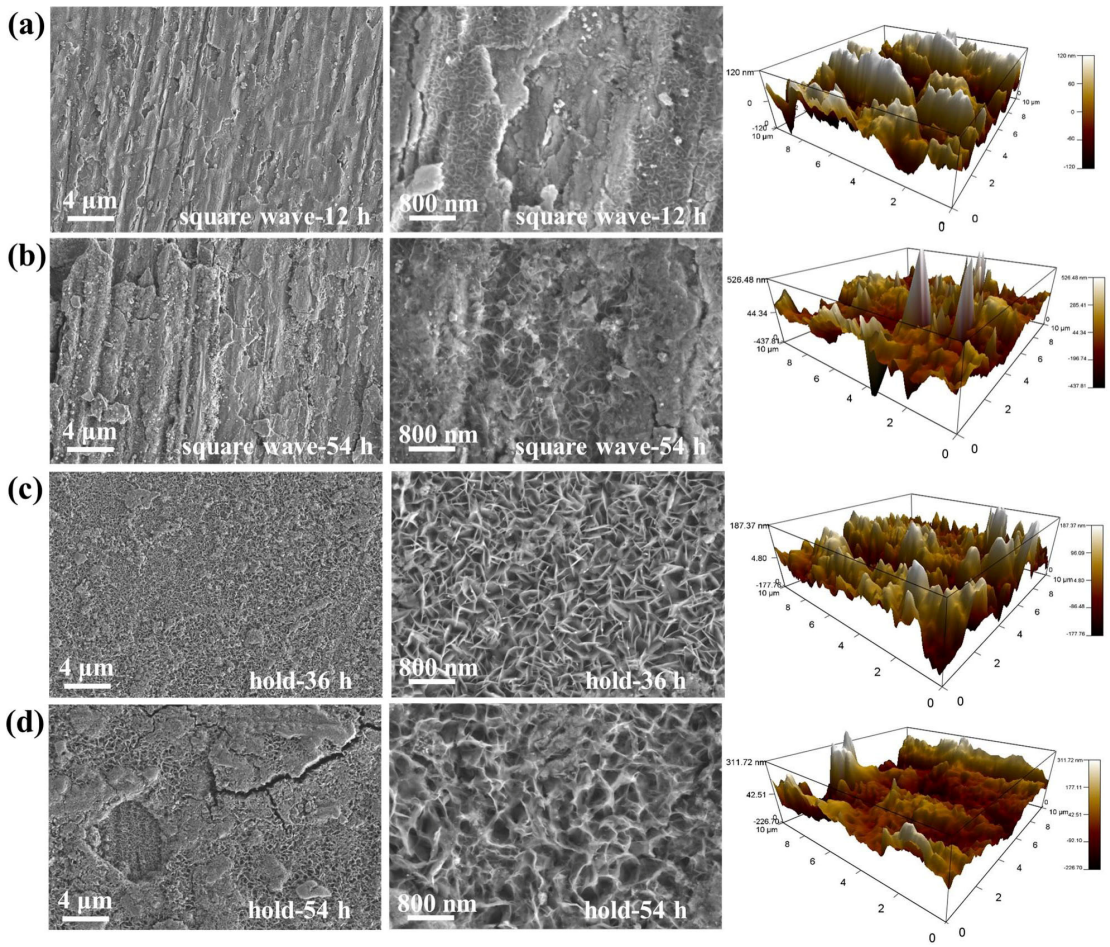

Figure 4. SEM and AFM images of plate Ni cathode. (**a**) Optimal performance with square-wave voltage. (**b**) End of test with square-wave voltage. (**c**) Optimal performance with holding voltage. (**d**) End of test under holding voltage.

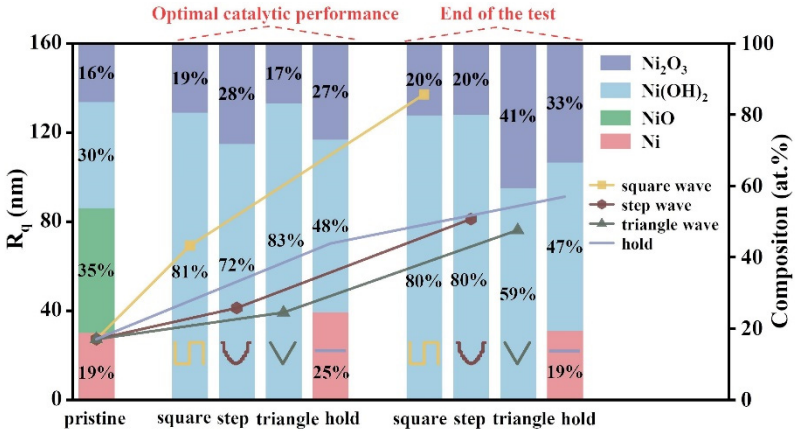

Figure 5. XPS and AFM results for plate Ni cathode.

2.2. Effect of Voltage Fluctuation Amplitude on Electrode Degradation and HER Performance

2.2.1. Time–Current Density Curves of FeNiMo-LDH@NiMo/SS with Fluctuating Power for HER

In recent years, to enhance the performance of cathodic materials and reduce costs, coating electrodes have commonly been prepared through electroplating or spraying methods. Layered double hydroxide (LDH) has become a research hotspot due to its unique electronic distribution, high specific surface area, and layered structure, leading to remarkable catalytic performance [23,55,58]. However, LDH-coated electrodes have some inherent disadvantages, such as operational damage and poor durability under harsh conditions [59,60]. In the previous Section 3.1, the effects of different voltage waveforms on the performance of plate Ni cathode were explored, among which the square-wave voltage had the strongest effect. The square-wave voltage represents intermittent outage when powered by renewable energy sources, which forces the electrode material to undergo continuous start–stop operations, which is an extremely demanding application environment for cathodic materials [61,62]. Renewable energies exhibit varying degrees of fluctuation in different seasons, times, and regions, potentially resulting in different levels of impact on electrode degradation and HER performance. Therefore, it is necessary to study the influence of square waves with different fluctuation amplitudes on the performance of an LDH electrode, which may expand the commercial applications of hydrogen production systems from electrolytic water.

In the following test, the working electrodes were FeNiMo-LDH@NiMo/SS-coated electrodes, which exhibited excellent HER catalytic performance in alkaline electrolyte, as demonstrated in Table 1. The fluctuation amplitudes of square-wave voltage were −1.275~0 V, −1.358~0 V and −1.592~0 V, respectively. These tests were completed for 180 h, and the T-I curves were recorded, as are shown in Figure S8. The current density was positively correlated with the input voltage. The current density results for all power fluctuation amplitudes presented a decreasing behavior during the test time, with larger fluctuations in voltage amplitudes resulting in a more pronounced decrease. The beginning of the test, intermediate point and end of the test T-I curves are enlarged and presented in Figure 6a–d, and the average current density for 6 h periods are given as statistics in Figure 7.

When the fluctuation amplitude was −1.275~0 V, for the first 2 h, the T-I curve exhibited an excellent response to the voltage fluctuation, and the current density reached 50 mA cm^{-2}@−1.275 V. The current density continually decreased to 38 mA cm^{-2}@−1.275 V after 180 h, with a decrease rate of 24% (Figures 6a and 7). The decrease in current density indicated the decline in catalytic activity and hydrogen evolution efficiency. When the fluctuation amplitudes were −1.358~0 V and −1.592~0 V, current densities reached 100 mA cm^{-2}@−1.358 V, and 200 mA cm^{-2}@−1.592 V in the first 2 h, respectively. Both current densities gradually declined during the test time and finally reached 43 mA cm^{-2}@−1.358 V (43 mA cm^{-2}@−1.592 V), with decrease rates of 57% and 79%, respectively. The

final current density values of the two were identical, possibly attributable to the loss of LDH structure on the electrode surface and the subsequent exposure of the NiMo coating. As the amplitude fluctuation increased, the decrease in the catalytic activity of FeNiMo-LDH@NiMo/SS became more pronounced. This provided evidence that a larger fluctuation range undermined the coating, resulting in a greater degradation in performance. As control tests, constant voltages of −1.275 V, −1.358 V, and −1.592 V were administered to the cathode, resulting in a slight reduction in current density with reduction rates of 11%, 19%, and 49%, respectively. FeNiMo-LDH@NiMo/SS exhibited decent stability at low holding voltages. The performance degradation caused by square-wave voltage was more pronounced compared to that of a constant voltage. These findings strongly suggested that large fluctuations exacerbated the detrimental impact on the catalytic behavior of the electrode.

Table 1. Comparison of HER catalysts in alkaline electrolyte.

HER Catalyst	Overpotential at 10 mA cm^{-2} (mV)	Ref.
FeNiMo-LDH@NiMo/SS	245	This work
Plate Ni cathode	430	This work
NF	378	[63]
SSFSe	237	[64]
SS Scrubber	418	[65]
SSM-Ni	346	[66]
NiP@SS	268	[67]
FeNi LDH/NF	315	[68]
TiC/NiSA	202	[69]
6-CMS	249	[63]
PtCoV/g-C_3N_4	346	[70]
$CoNi_{0.04}$-MOF-74/NF	203	[71]

An oxidation current was observed for each square-wave loop instant drop from the crest voltage to 0 V. During the first 2 h, the oxidation current density reached 50 mA cm^{-2} at −1.275~0 V. After 180 h, the oxidation current density decreased to 47 mA cm^{-2}. When the voltage amplitudes were −1.358~0 V and −1.592~0 V, respectively, the oxidation current density for the former decreased from 56 mA cm^{-2} (the first 2 h of the test) to 38 mA cm^{-2}, while the oxidation current density for the latter dropped from 71 mA cm^{-2} to 7 mA cm^{-2}. As the HER progressed, the oxidation current density decreased. The decrease in the oxidation current density was attributed to the oxidation of the catalytically active substance FeNiMo-LDH@NiMo/SS, leading to a reduction in its catalytic activity. The exposure to a higher amplitude of voltage fluctuation precipitated the increase in oxidation current density. Therefore, the oxidization degree of FeNiMo-LDH@NiMo/SS was augmented with the increase in fluctuation range. This resulted in a greater degradation of performance and durability. The oxidation current was primarily attributed to the reverse redox reaction of the electrode material, with the active substance on the electrode surface serving as the main driving force for this phenomenon [40]. The rapid decrease in the oxidation current density at a high fluctuation amplitude also implied that the active material on the surface of FeNiMo-LDH@NiMo/SS was being depleted. Therefore, it seemed that there was a mutually influential relationship between the oxidation current and the active substance. Specifically, the oxidation current diminished the active material on the FeNiMo-LDH@NiMo/SS surface, resulting in a reduction in the oxidation density generated by FeNiMo-LDH@NiMo/SS. To sum up, the magnitude of the oxidation current density is affected by the fluctuation amplitude and the active substance. The type and the content of active substance on the electrode's surface control the oxidation current behavior. The oxidation current causes oxidation of the cathode's active substance, thus reducing the oxidation current density, ultimately resulting in a decline in HER electrode performance.

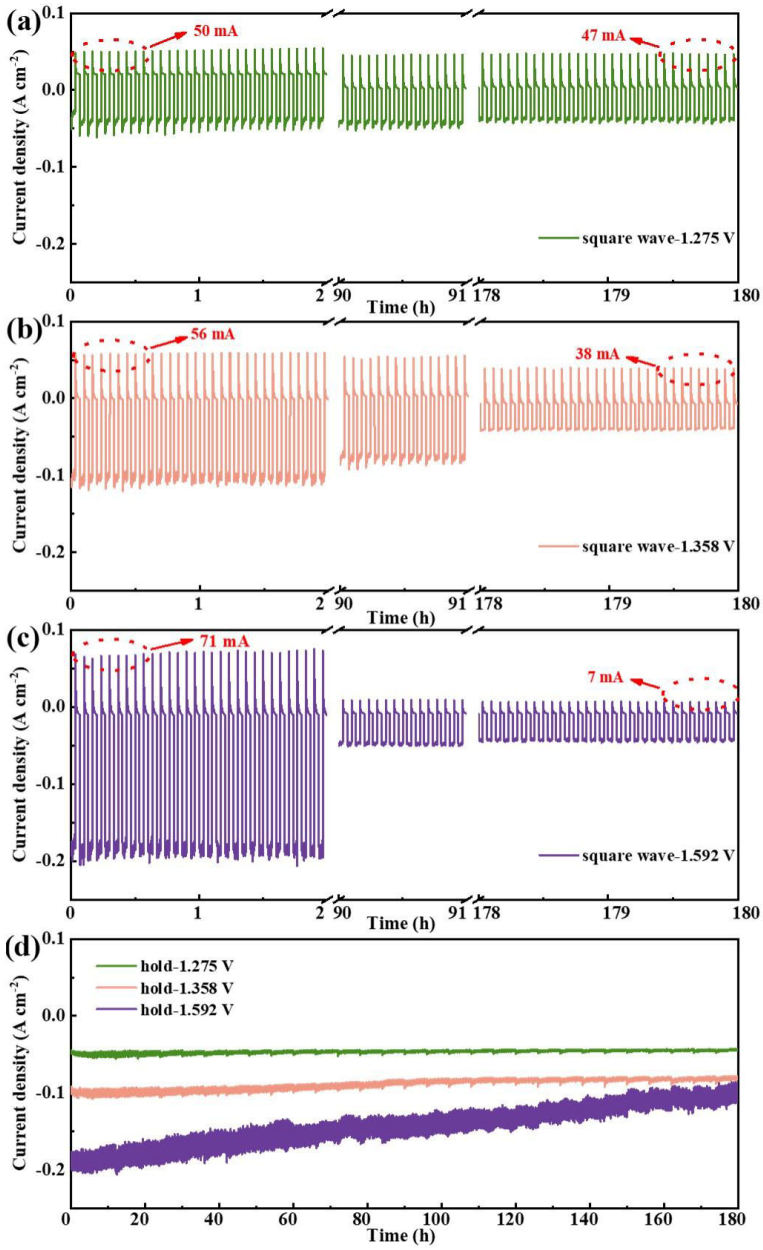

Figure 6. T–I curves of FeNiMo-LDH@NiMo/SS in 1.0 mol L^{-1} NaOH solution at 80 °C. Powered by (**a**) −1.275~0 V in square wave; (**b**) −1.358~0 V in square wave; (**c**) −1.592~0 V in square wave; and (**d**) −1.275 V, −1.358 V and −1.592 V in holding voltage.

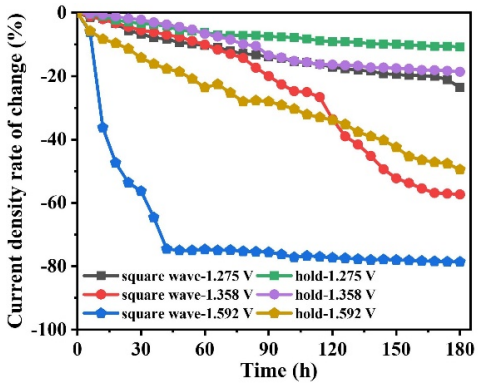

Figure 7. The relationship between the current density change rate and time.

2.2.2. HER Performance Test

To investigate the power fluctuation amplitude's impact on the HER performance of FeNiMo-LDH@NiMo/SS, the LSV curve was employed to enable us to investigate the HER performance of FeNiMo-LDH@NiMo/SS with various fluctuation amplitudes of voltage. The original data of the LSV test results are shown in Figure S9, and the statistical results are presented in Figure 8.

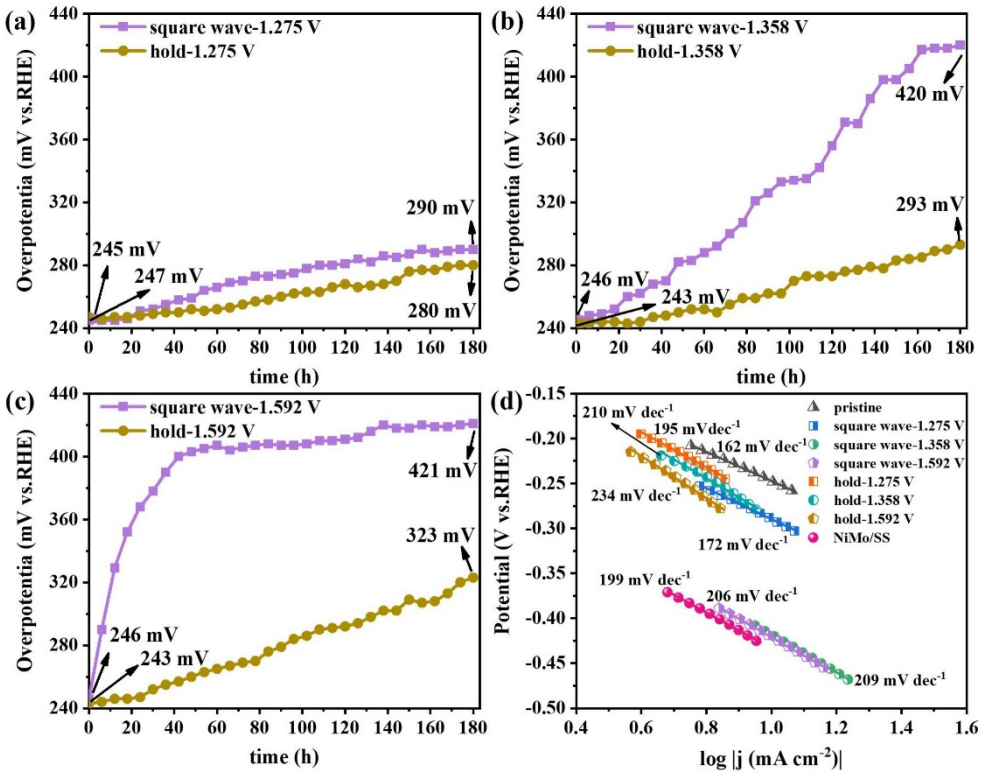

Figure 8. Overpotential (10 mA cm^{-2}) at (**a**) −1.275 V (hold) and −1.275~0 V (square wave); (**b**) −1.358 V (hold) and −1.358~0 V (square wave); and (**c**) −1.592 V (hold) and −1.592~0 V (square wave). (**d**) Tafel slopes.

According to Figures 8 and S9, the shift in LSV curves and the change in overpotential to reach a geometric current density of 10 mA cm^{-2} showed similar trends with various fluctuation amplitudes, and both parameters demonstrated a continuous upward trend. The observed trend differed from that of plate Ni cathodes because under fluctuating power conditions, FeNiMo-LDH@NiMo/SS failure involved not only a compositional change in the electrode's surface and degradation of the surface area but also detachment of the LDH layer. For FeNiMo-LDH@NiMo/SS with square-wave power (−1.275 to 0 V), the initial overpotential was 245 mV, which significantly increased to 290 mV after 180 h of testing. When the voltage fluctuation amplitudes were −1.358~0 V and −1.592~0 V, respectively, the overpotential for the former rapidly increased to 417 mV after 162 h, while the overpotential for the latter exhibited a sharp increase to 400 mV after 42 h. Subsequently, both of them slowly increased to approximately 420 mV over a period of 180 h. These results indicated the reduced HER activity of the coated electrode with fluctuating power. A larger fluctuation amplitude notably accelerated the deterioration of the electrode surface, resulting in greater performance and durability losses. After operating for 180 h within the fluctuation ranges of −1.358~0 V and −1.592~0 V, the overpotential of FeNiMo-LDH@NiMo/SS (420 mV) fell between those of Ni/SS (440 mV) and NiMo/SS (292 mV) (Figure S10). This suggested that detachment of the FeNiMo-LDH and NiMo coatings from the surface of FeNiMo-LDH@NiMo/SS may have occurred, leading to the exposure of a portion of the NiMo coating. In contrast, the overpotential change in FeNiMo-LDH@NiMo/SS with three

holding voltages was also measured, which showed a gradual increase over the test time. After 180 h of testing with the voltage held constant, the overpotential increase was smaller than that for the square wave, further demonstrating that voltage fluctuation significantly impacted the stability of FeNiMo-LDH@NiMo/SS electrocatalytic performance. The presence of power fluctuations can result in a decline in performance, while a high amplitude of these fluctuations further accelerates the degradation process of the active layer [42] and causes the catalyst to be oxidized and separate from the substrate. Therefore, implementing effective measures to reduce voltage fluctuations during the production of hydrogen from renewable energy sources may serve as an effective system control strategy. The Tafel slope was generated after testing to further our understanding of the HER behavior of FeNiMo-LDH@NiMo/SS. For FeNiMo-LDH@NiMo/SS, the overpotential was 162 mV dec-1 at the beginning of the test. After 180 h, the Tafel slope of FeNiMo-LDH@NiMo/SS increased to 172 mV dec^{-1} (−1.275~0 V), 209 mV dec^{-1} (−1.358~0 V), and 206 mV dec^{-1} (−1.592~0 V), respectively, following the square-wave voltage test. The Tafel slope of FeNiMo-LDH@NiMo/SS after 180 h HER in the ranges of −1.358~0 V and −1.592~0 V was comparable to that of NiMo/SS (199 mV dec^{-1}). The aforementioned results indicated that the degradation of electrode performance was exacerbated by increasing the amplitude of voltage fluctuation. A large fluctuation amplitude caused detachment of the FeNiMo-LDH coating, revealing the underlying NiMo coating on the electrode surface. In summary, the effectiveness of hydrogen evolution on FeNiMo-LDH@NiMo/SS is significantly influenced by the magnitude of fluctuation. A high amplitude of fluctuation accelerates the degradation of the LDH structure, resulting in its release from the matrix.

2.2.3. Surface Characterizations of FeNiMo-LDH@NiMo/SS with Fluctuating Power

Surface analysis measurements, via SEM, EDS and XPS, were performed on FeNiMo-LDH@NiMo/SS with different fluctuation amplitudes at the beginning and at the end of the test. As a control test, surface characterizations were also made of FeNiMo-LDH@NiMo/SS with the holding voltage.

As shown in Figure S11, the NiMo film on the surface of NiMo/SS had a spherical structure. The surface coating of FeNiMo-LDH@NiMo/SS was dense and consisted of spherical particles arranged in a flower-like structure (Figure S12). The flower–ball structures were composed of uniformly distributed nanosheets, displaying a typical layered structure that conferred excellent catalytic activity to FeNiMo-LDH@NiMo/SS. From the EDS spectrum of the FeNiMo-LDH@NiMo/SS electrode, it is evident that Fe, Ni, and Mo elements are present on the electrode surface. Fe and Ni are evenly distributed on the surface of the electrode, while Mo is primarily concentrated in the flower-like structure. When exposed to a square-wave voltage of −1.275~0 V for a duration of 180 h (Figure 9a), FeNiMo-LDH@NiMo/SS exhibited a significant decrease in the abundance of its flower-shaped spherical structures, accompanied by an uneven distribution and the appearance of a few spherical structures. Under magnification, it became evident that the flower-shaped spherical structures underwent a notable reduction in size. FeNiMo-LDH@NiMo/SS suffered more severe damage when subjected to a wider fluctuation amplitude of square-wave voltage (−1.358~0 V). The flower-like spherical structures were significantly reduced (Figure 9b), and disordered strip structures emerged as a result. Furthermore, when applying a fluctuation amplitude range from −1.592 to 0 V (Figure 9c), the surface morphology of FeNiMo-LDH@NiMo/SS appeared disordered, with the disappearance of flower-like spherical structures and the presence of large block and strip structures. When we amplified the fluctuation amplitude, FeNiMo-LDH@NiMo/SS suffered significant surface damage. The observation of the uneven distribution of Fe, Ni, and Mo elements in the EDS results further confirms the detrimental impact of power fluctuations on the catalytic structure of the electrode surface (Figure S13). The catalytic activity of the electrode is primarily associated with its LDH structure, and so its performance degradation was attributed to the disruptive effects of power fluctuations on its LDH structure, leading to a reduction in the number of catalytically active sites. Therefore, with an increase in the fluctuation

amplitude, the electrode's performance deteriorated rapidly. The presence of spherical structures indicated the exposure of the NiMo film, resulting from the dissolution of the active substance. The repeated occurrence of an oxidation current resulted in the continuous dissolution and deposition of the catalytic substance, and then the diameter of the flower-shaped spherical structure was reduced. Consequently, the electrode's performance and durability were severely compromised, particularly under conditions of high fluctuation amplitudes. Regarding the electrode under the holding voltage, there was only a slight change in surface morphology observed on the cathode. Hence, research into a highly adhesive coating electrode holds significant potential for harnessing solar energy efficiently.

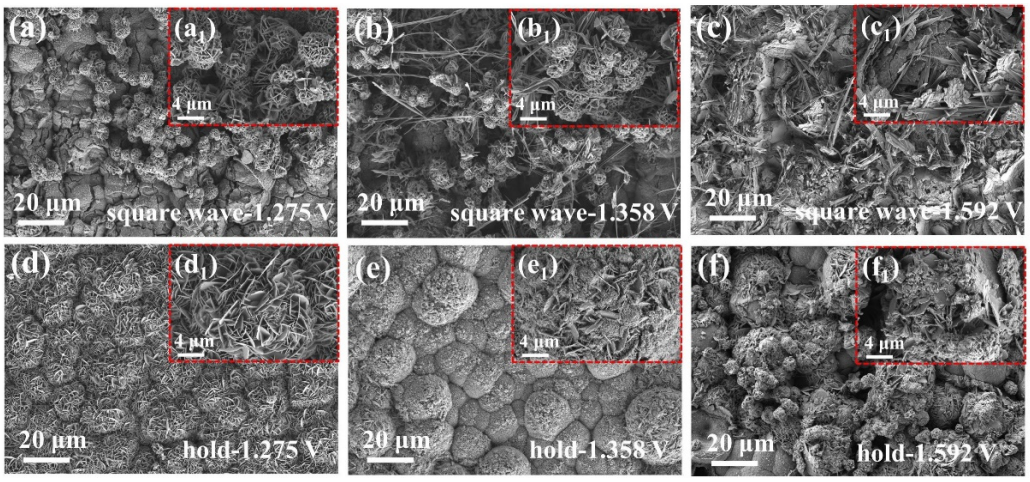

Figure 9. SEM images of FeNiMo-LDH@NiMo/SS. (**a**) −1.275~0 V in square wave. (**b**) −1.358~0 V in square wave. (**c**) −1.592~0 V in square wave. (**d**) −1.275 V in holding voltage. (**e**) −1.358 V in holding voltage. (**f**) −1.592 V in holding voltage.

The spectral survey results (Figure S14) revealed the presence of Fe^{3+}, Ni^{2+}, and Mo^{6+} on the pristine FeNiMo-LDH@NiMo/SS surface, which was consistent with the findings of previous studies. After the square-wave test, characteristic peaks indicating the generation of Ni^{3+} and Fe^{2+} at FeNiMo-LDH@NiMo/SS were observed, as shown in Figure S15, while these peaks were not observed during the voltage hold test. This demonstrated that under fluctuating power conditions during the HER process, oxidation currents were generated at FeNiMo-LDH@NiMo/SS, leading to frequent oxidation–reduction reactions. By calculating the relative content of each element (as shown in Figure 10), we found that within a voltage range of −1.275~0 V, the relative contents of Ni^{3+} and Fe^{2+} were 16% and 8%, respectively. With an increasing fluctuation amplitude, these values slightly increased. When the fluctuation ranges were −1.358~0 V and −1.592~0 V, respectively, the relative contents increased to 17% and 18% for Ni^{3+}, as well as 10% and 12% for Fe^{2+}. The relative content of Mo^{6+} decreased from 24% for pristine FeNiMo-LDH@NiMo/SS to 9% (−1.275~0 V), 10% (−1.358~0 V) and 3% (−1.592~0 V), respectively. As fluctuation amplitude increased further, the relative contents of Ni^{3+} and Fe^{2+} also increased, correspondingly promoting higher degrees of electrode oxidation reaction. This phenomenon could be attributed to the augmentation of the oxidation current caused by the enlarged fluctuation amplitude, resulting in electrode dissolution and a decreased performance level. Simultaneously, increasing the amplitude led to a rapid decrease in Mo content, which was not conducive to water dissociation and increased the hydrogen adsorption free energy, thereby reducing the hydrogen evolution performance [61,72]. Therefore, it seems that the catalytic performance of FeNiMo-LDH@NiMo/SS is also affected by a decreased Mo content. Increasing the fluctuation amplitude significantly accelerates the degradation process, resulting in higher performance losses along with a decline in durability.

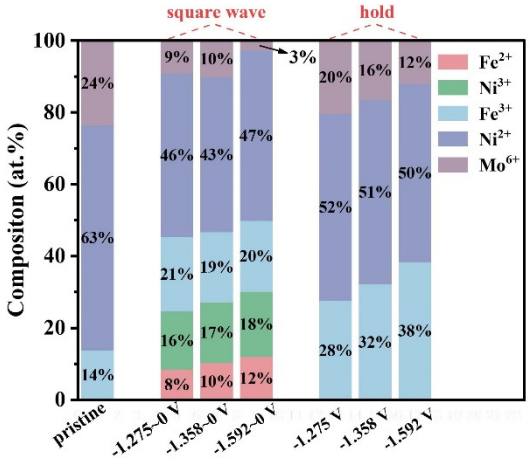

Figure 10. XPS results for surface chemical analysis of FeNiMo-LDH@NiMo/SS.

3. Experimental Section

3.1. Materials

A pure nickel coupon and FeNiMo-LDH@NiMo/SS were used as the study HER cathode for this work. The size of the nickel coupon was 20 mm × 13 mm × 2 mm, and the chemical composition was as follows: Ni > 99.90%, Cu 0.01%, Si 0.01%, Mn < 0.01%, Fe 0.01%, Zn < 0.005% and Cd < 0.002%. We utilized 304 stainless steel (40 mm × 13 mm × 2 mm, wt%: P 0.04, Ni 11.00, Si 1.00, S 0.03, Cr 19.00, C 0.08, Mn 2.00, Fe bal.) as the substrate for FeNiMo-LDH@NiMo/SS.

Sodium citrate dihydrate ($Na_3(C_6H_5O_7)\cdot 2H_2O$, AR), sodium molybdate dihydrate ($Na_2MoO_4\cdot 2H_2O$, AR), ammonia solution (NH_4OH, 25–28 wt%) and nickel chloride hexahydrate ($NiCl_2\cdot 6H_2O$, AR) were purchased from the Aladdin Biochemical Technology Co., Ltd., Shanghai, China. Urea ($CO(NH_2)_2$, AR), nickel sulfate hexahydrate ($NiSO_4\cdot 6H_2O$, AR), ethanol (C_2H_5OH, AR), hydrochloric acid (HCl, 36–38 wt%), ferric nitrate nonahydrate (Fe $(NO_3)_3\cdot 9H_2O$, AR), sodium hydroxide (NaOH, AR), and ammonium fluoride (NH_4F, AR) were purchased from the Chengdu Kelong Chemical Reagent Factory, Chengdu, China. The deionized water (RO, III) used in the experiments was prepared using an ultrapure purification system purchased from Chengdu Youpu Ultrapure Technology Co., Ltd., Chengdu, China. The chemicals used in this study were not purified further.

3.2. HER Electrode Preparation

Pure Ni coupon cathodes were polished with SiC papers (grades 280 to 2000) and then cleaned with deionized water, acetone, and ethanol, in that order. Then, they were placed in an airtight box until use.

FeNiMo-LDH@NiMo/SS was prepared using electrodeposition and the hydrothermal method, as previously reported [23]. The pre-treatment of 304 stainless steels followed the same steps as above. Prior to electrodeposition, pre-nickel electrodeposition was performed to activate the surface of the steel, to produce a uniformly dense and highly cohesive NiMo film for LDH growth. Then, the NiMo/SS electrode was prepared using electrodeposition. Finally, highly crystalline FeNiMo-LDH@NiMo/SS was synthesized via the hydrothermal method.

3.3. HER Performance and Durability Test for Electrode under Fluctuating Power

The performance and durability of the HER electrode were comprehensively evaluated using a series of electrochemical techniques, including time (T)–current density (I) curves, linear sweep voltammetry (LSV), cyclic voltammetry (CV), and electrochemical impedance spectroscopy (EIS). The T-I curve test assesses the dynamic response and hydrogen evolution performance of the electrode, while the LSV test measures the hydrogen evolution activity. Additionally, the CV test examines the electrochemically active surface

area (ECSA), and the EIS test reveals the interface properties. Integrating these methodologies provided a comprehensive understanding of the HER electrode's performance under fluctuating electrical conditions, offering valuable insights for research and development in renewable energy applications.

In this study, the input voltage simulated the characteristics of solar power generation to obtain the T-I curve. The input voltage waves were square, step, triangle, and hold, and the voltage period was 240 s, as shown in Figure 11. The square-wave voltage was operated at a negative voltage (V_{HER}) for 120 s. In the step-wave voltage, the 240 s period was divided into 13 equal parts, and for each of those, we operated at a different voltage. The triangle-wave voltage was reduced from 0 V to V_{HER} in 120 s at a constant rate, and it was increased to 0 V in 120 s at the same rate. The holding voltage operated at a negative voltage (V_{HER}).

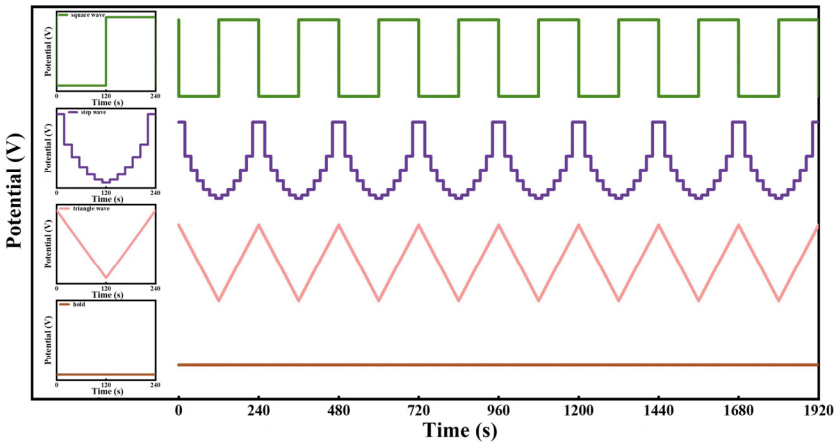

Figure 11. Evolution of voltage as a function of time.

In conventional three-electrode cells, HER performance and durability tests were conducted using a CHI660E electrochemical workstation. All measurements were carried out in a laboratory environment with 1.0 mol L^{-1} NaOH solution at 80 °C. A plate Ni cathode and FeNiMo-LDH@NiMo/SS were used as the working electrodes, with a 1 cm^2 area exposed to the electrolyte. A Hg/HgO electrode and platinum sheet were used as the reference electrode and counter electrode, respectively. In order to simulate water electrolysis for green hydrogen under the condition of electric power fluctuation, the input voltage (V_{HER}) was the average voltage at a certain current density. To simulate the flow of the electrolytic water process in the industry, the electrolyte was agitated at a speed of 1300 rpm min^{-1}. All measured potentials were converted to the reversible hydrogen electrode (RHE) using the following relationship:

$$E_{RHE} = E_{Hg/HgO} + 0.059pH + 0.098 \quad (3)$$

where 0.098 was the standard electrode potential of the Hg/HgO reference electrode.

Linear scan voltammogram (LSV) polarization curves were obtained at a scan rate of 5 mV s^{-1}. The Tafel slope was calculated from the LSV curves, and the overpotential (η) at the corresponding current density was calculated using the above relationship. Electrochemical impedance spectroscopy (EIS) was measured from 10^5–10^{-2} Hz at an amplitude of 5 mV. The cyclic voltammogram (CV) curves were obtained at different sweep rates (10, 20, 30, 40, 50, 60, 70, and 80 mV s^{-1}) in the region of 0.1 to 0.3 V_{RHE}, and the double-layer capacitance (C_{dl}) was calculated from the CV curve.

3.4. Characterization

After various electrochemical tests, all samples were rinsed with deionized water, followed by cold-air drying and subsequent storage in a super-purified glove box to ensure

that they were exposed to the ambient environment for less than 3 min before observations for characterization.

Scanning electron microscopy (SEM, Gemini 300 ZEISS, Oberkochen, Germany) was used to characterize the morphologies at an accelerating voltage of 3 kV. The distribution of elements on the electrode surface were measured using an energy dispersion spectrometer (EDS, OXFORD Xplore, Oberkochen, Germany) equipped with SEM.

The surface roughness of the electrodes was determined using atomic force microscopy (AFM, MFP 3D Bio, Abingdon, UK) at a scan size of 10×10 μm^2. For each surface, AFM images sized 256×256 pixels were obtained.

The electron valence states on the electrode surfaces were investigated by using X-ray photoelectron spectroscopy (XPS, Thermo Scientific K-Alpha, Waltham, MA, USA). In this XPS, the diffraction source was an Al Kα ray ($h\nu$ = 1486.6 eV), the working voltage was 12 kV, and the filament current was 6 mA. The obtained XPS data were processed using Thermo Advantage software version 5.948. The chemical compositions on the surfaces of the electrodes were calculated using the convolution method with a sensitivity factor [73]. Equation (4) was used to calculate the composition (at%, C_x)) of the relative contents:

$$C_x = \frac{(I_x/S_x)}{\sum(I_x/S_x)} \quad (4)$$

where S_x is the sensitivity factor based on the XPS instrument, and I_x is the peak intensity corresponding to the area of the element.

4. Conclusions

In this work, three wave shapes (square, step, and triangle) were used to simulate renewable energies for the HER process. Fluctuating power led to the HER performance of the plate Ni cathode increasing at first and then slightly decreasing. The fluctuating power enhanced the oxidation state of the cathode surface and led to a decline in the active sites. At the same time, the degradation of the cathode surface resulted in an increase in the surface area. Square power had the strongest effect on HER performance, which led the plate Ni cathode to reach the strongest HER performance in 12 h with the optimum catalytic parameters. This was followed by the step and triangle powers, respectively. The square voltage with various amplitudes was then administered to a plate-like FeNiMo-LDH@NiMo/SS cathode. As the amplitude increased, the LDH-coated cathode showed an accelerating degradation, mainly due to the separation of the catalytic active sites. For dynamic investigations, further relevant studies will be conducted, such as the analysis of voltage fluctuation frequency and voltage change rate. In addition, it seems that the appearance of an oxidation current when there is a fluctuating voltage plays a key role in the degradation process of the cathode, which should be further explored. In those regards, this research provides a method for evaluating the cathode HER performance and degradation behavior in scenarios of generating green hydrogen from renewable energies, a contribution that will help to guide the development of the hydrogen industry.

Supplementary Materials: The following supporting information can be downloaded at https://www.mdpi.com/article/10.3390/catal14050307/s1, Figure S1: T–I curves of plate Ni cathode in 1.0 mol L^{-1} NaOH solution at 80 °C, (a) Powered by square wave voltage, (b) Step wave, (c) Triangle wave, (d) The relationship between the current density change rate and time; Figure S2: LSV curves of the Ni cathode with fluctuation power, (a) Square wave, (b) Step wave, (c) Triangle wave, (d) Hold; Figure S3: Linear regression fitting was conducted to determine the C_{dl}, (a) Square wave, (b) Step wave, (c) Triangle wave, (d) Hold; Figure S4: The Tafel slope value at the pristine state, optimal performance and at the end of the test, (a) Square wave, (b) Step wave, (c) Triangle wave, (d) Hold; Figure S5: Nyquist plots for EIS, (a) Square wave, (b) Step wave, (c) Triangle wave, (d) Hold, (e) Equivalent electrical circuit diagram; Figure S6: SEM and AFM images of plate Ni cathode, (a) Pristine, (b) Optimal performance with step wave voltage, (c) End of test with step wave voltage, (d) Optimal performance with triangle wave voltage, (e) End of test with triangle wave voltage;

Figure S7: XPS surface chemical analyses of plate Ni cathode, (a) Optimal performance, (b) End of the test; Figure S8: T–I curves of FeNiMo-LDH@NiMo/SS for square wave test in 1.0 mol L^{-1} NaOH solution at 80 °C, (a) −1.275~0 V. (b) −1.358~0 V, (c) −1.592~0 V; Figure S9: LSV curves of FeNiMo-LDH@NiMo/SS, (a) −1.275~0 V in square wave, (b) −1.275 V in holding voltage, (c) −1.358~0 V in square wave, (d) −1.358 V in holding voltage, (e) −1.592~0 V in square wave, (f) −1.592 V in holding voltage; Figure S10: Electrocatalytic HER performance of three catalytic electrodes, (a) LSV curves, (b) The overpotential at 10 mA cm^{-2}; Figure S11: SEM images of NiMo/SS, (a) 20 μm, (b) 2 μm; Figure S12: SEM images of pristine FeNiMo-LDH@NiMo/SS, (a) 20 μm, (b) 2 μm, (c) EDS images of Fe, Ni and Mo; Figure S13: EDS images of FeNiMo-LDH@NiMo/SS, (a) −1.275~0 V in square wave, (b) −1.358~0 V in square wave, (c) −1.592~0 V in square wave, (d) −1.275 V in holding voltage, (e) −1.358 V in holding voltage, (f) −1.592 V in holding voltage; Figure S14: XPS surface chemical analyses of pristine FeNiMo-LDH@NiMo/SS, (a) Wide-scan XPS spectra, (b) Fe 2p, (c) Ni 2p, (d) Mo 3d; Figure S15: XPS surface chemical analyses of FeNiMo-LDH@NiMo/SS, (a) Fe 2p in square wave, (b) Fe 2p in holding voltage, (c) Ni 2p in square wave, (d) Ni 2p in holding voltage, (e) Mo 3d in square wave, (f) Mo 3d in holding voltage; Table S1: The variations of solution resistance (R_s), charge transfer resistance (R_{ct}) and R_1.

Author Contributions: Conceptualization, B.L., H.W., J.T. and C.Z. formal analysis, C.L.; investigation, C.L.; writing—original draft preparation, C.L.; writing—review and editing, B.L., H.Z. and Y.W.; supervision, B.L., H.W. and J.T.; project administration, H.Z.; funding acquisition, J.T. All authors have read and agreed to the published version of the manuscript.

Funding: This research was funded by the Scientific and Technological Innovation Project of Laoshan Lab, grant number No. LSKJ202205700. And the study was funded by the Key R&D Program of the Science and Technology Department of Sichuan Province (No. 2021ZYCD003), the Major Science and Technology Project of the CNPC (No. 2022DJ3211) and the Science and Technology Project of Southwest Petroleum University (No. 2021JBGS05).

Data Availability Statement: The data presented in this study are available on request from the corresponding author. The data are not publicly available due to privacy.

Conflicts of Interest: The authors declare that this study received funding from CNPC Shenzhen New Energy Research Institute of company Co., Ltd. J.T. had the following involvement with the study: Conceptualization, Supervision, Funding acquisition.

References

1. Liu, H.; Ampah, J.D.; Zhao, Y.; Sun, X.; Xu, L.; Jiang, X.; Wang, S. A Perspective on the Overarching Role of Hydrogen, Ammonia, and Methanol Carbon-Neutral Fuels towards Net Zero Emission in the Next Three Decades. *Energies* **2023**, *16*, 280. [CrossRef]
2. Kojima, H.; Nagasawa, K.; Todoroki, N.; Ito, Y.; Matsui, T.; Nakajima, R. Influence of renewable energy power fluctuations on water electrolysis for green hydrogen production. *Int. J. Hydrogen Energy* **2023**, *48*, 4572–4593. [CrossRef]
3. Caldeira, K.; Jain, A.K.; Hoffert, M.I. Climate Sensitivity Uncertainty and the Need for Energy Without CO_2 Emission. *Science* **2003**, *299*, 2052–2054. [CrossRef] [PubMed]
4. Sayed, E.T.; Olabi, A.G.; Alami, A.H.; Radwan, A.; Mdallal, A.; Rezk, A.; Abdelkareem, M.A. Renewable Energy and Energy Storage Systems. *Energies* **2023**, *16*, 1415. [CrossRef]
5. Zou, X.; Zhang, Y. Noble metal-free hydrogen evolution catalysts for water splitting. *Chem. Soc. Rev.* **2015**, *44*, 5148–5180. [CrossRef] [PubMed]
6. Acar, C.; Dincer, I. The potential role of hydrogen as a sustainable transportation fuel to combat global warming. *Int. J. Hydrogen Energy* **2020**, *45*, 3396–3406. [CrossRef]
7. Chatenet, M.; Pollet, B.G.; Dekel, D.R.; Dionigi, F.; Deseure, J.; Millet, P.; Braatz, R.D.; Bazant, M.Z.; Eikerling, M.; Staffell, I.; et al. Water electrolysis: From textbook knowledge to the latest scientific strategies and industrial developments. *Chem. Soc. Rev.* **2022**, *51*, 4583–4762. [CrossRef] [PubMed]
8. Glenk, G.; Reichelstein, S. Economics of converting renewable power to hydrogen. *Nat. Energy* **2019**, *4*, 216–222. [CrossRef]
9. Li, L.; Liu, Y.; Lin, B.; Wang, Y.; Song, K.; Zhang, H.; Li, Y.; Li, J.; Zheng, H.; Tang, J.; et al. Properties, mechanisms and advantages of metallic glass for electrocatalysis and HER in water splitting: A review. *Int. J. Hydrogen Energy* **2023**, *48*, 27182–27200. [CrossRef]
10. Yang, W.; Chen, S. Recent progress in electrode fabrication for electrocatalytic hydrogen evolution reaction: A mini review. *Chem. Eng. J.* **2020**, *393*, 124726. [CrossRef]
11. Raveendran, A.; Chandran, M.; Dhanusuraman, R. A comprehensive review on the electrochemical parameters and recent material development of electrochemical water splitting electrocatalysts. *RSC Adv.* **2023**, *13*, 3843–3876. [CrossRef]
12. Thoi, V.S.; Sun, Y.; Long, J.R.; Chang, C.J. Complexes of earth-abundant metals for catalytic electrochemical hydrogen generation under aqueous conditions. *Chem. Soc. Rev.* **2013**, *42*, 2388–2400. [CrossRef] [PubMed]

13. Debe, M.K. Electrocatalyst approaches and challenges for automotive fuel cells. *Nature* **2012**, *486*, 43–51. [CrossRef]
14. Mohana, P.; Isacfranklin, M.; Yuvakkumar, R.; Ravi, G.; Kungumadevi, L.; Arunmetha, S.; Han, J.H.; Hong, S.I. Facile Synthesis of Ni-MgO/CNT Nanocomposite for Hydrogen Evolution Reaction. *Nanomaterials* **2024**, *14*, 280. [CrossRef] [PubMed]
15. Shamskhou, K.; Awada, H.; Yari, F.; Aljabour, A.; Schöfberger, W. A Molecular Binuclear Nickel (II) Schiff Base Complex for Efficient HER Electrocatalysis. *Catalysts* **2023**, *13*, 1348. [CrossRef]
16. Ash, P.A.; Vincent, K.A. Spectroscopic analysis of immobilised redox enzymes under direct electrochemical control. *Chem. Commun.* **2012**, *48*, 1400–1409. [CrossRef] [PubMed]
17. Wan, Z.; Tang, P.; Dai, L.; Yang, Y.; Li, L.; Liu, J.; Yang, M.; Deng, G. Highly Effective Electrochemical Water Splitting with Enhanced Electron Transfer between Ni_2Co Layered Double Hydroxide Nanosheets Dispersed on Carbon Substrate. *C* **2023**, *9*, 94. [CrossRef]
18. Wu, T.; Sun, M.; Wong, H.H.; Chan, C.H.; Lu, L.; Lu, Q.; Chen, B.; Huang, B. Recent advances and strategies of electrocatalysts for large current density industrial hydrogen evolution reaction. *Inorg. Chem. Front.* **2023**, *10*, 4632–4649. [CrossRef]
19. Che, Q.; Li, Q.; Tan, Y.; Chen, X.; Xu, X.; Chen, Y. One-step controllable synthesis of amorphous (Ni-Fe)S_x/NiFe$(OH)_y$ hollow microtube/sphere films as superior bifunctional electrocatalysts for quasi-industrial water splitting at large-current-density. *Appl. Catal. B Environ.* **2019**, *246*, 337–348. [CrossRef]
20. Liang, H.; Xu, M.; Asselin, E. Corrosion of monometallic iron- and nickel-based electrocatalysts for the alkaline oxygen evolution reaction: A review. *J. Power Sources* **2021**, *510*, 230387. [CrossRef]
21. Wu, Z.P.; Lu, X.F.; Zang, S.Q.; Lou, X.W. Non-noble-metal-based electrocatalysts toward the oxygen evolution reaction. *Adv. Funct. Mater.* **2020**, *30*, 1910274. [CrossRef]
22. Li, Y.; Zhang, G.; Lu, W.; Cao, F. Amorphous Ni–Fe–Mo Suboxides Coupled with Ni Network as Porous Nanoplate Array on Nickel Foam: A Highly Efficient and Durable Bifunctional Electrode for Overall Water Splitting. *Adv. Sci.* **2020**, *7*, 1902034. [CrossRef]
23. Jia, X.; Wang, Y.; Tang, J.; Song, K.; Zhang, H.; Lin, B.; Zheng, H. FeNi-LDH@Ni film modified stainless-steel as self-supported electrodes for efficient and stable overall water splitting in alkaline environments. *Surf. Coat. Technol.* **2023**, *464*, 129502. [CrossRef]
24. Wang, C.; Shang, H.; Jin, L.; Xu, H.; Du, Y. Advances in hydrogen production from electrocatalytic seawater splitting. *Nanoscale* **2021**, *13*, 7897–7912. [CrossRef] [PubMed]
25. Zhai, W.; Ma, Y.; Chen, D.; Ho, J.C.; Dai, Z.; Qu, Y. Recent progress on the long-term stability of hydrogen evolution reaction electrocatalysts. *InfoMat* **2022**, *4*, e12357. [CrossRef]
26. Anantharaj, S.; Ede, S.R.; Sakthikumar, K.; Karthick, K.; Mishra, S.; Kundu, S. Recent Trends and Perspectives in Electrochemical Water Splitting with an Emphasis on Sulfide, Selenide, and Phosphide Catalysts of Fe, Co, and Ni: A Review. *ACS Catal.* **2016**, *6*, 8069–8097. [CrossRef]
27. Wang, X.; Li, W.; Xiong, D.; Petrovykh, D.Y.; Liu, L. Bifunctional Catalysts: Bifunctional Nickel Phosphide Nanocatalysts Supported on Carbon Fiber Paper for Highly Efficient and Stable Overall Water Splitting (Adv. Funct. Mater. 23/2016). *Adv. Funct. Mater.* **2016**, *26*, 4066. [CrossRef]
28. Kitiphatpiboon, N.; Chen, M.; Li, X.; Liu, C.; Li, S.; Wang, J.; Peng, S.; Abudula, A.; Guan, G. Heterointerface engineering of Ni_3S_2@NiCo-LDH core-shell structure for efficient oxygen evolution reaction under intermittent conditions. *Electrochim. Acta* **2022**, *435*, 141438. [CrossRef]
29. Kuroda, Y.; Nishimoto, T.; Mitsushima, S. Self-repairing hybrid nanosheet anode catalysts for alkaline water electrolysis connected with fluctuating renewable energy. *Electrochim. Acta* **2019**, *323*, 134812. [CrossRef]
30. Alia, S.M.; Stariha, S.; Borup, R.L. Electrolyzer durability at low catalyst loading and with dynamic operation. *J. Electrochem. Soc.* **2019**, *166*, F1164. [CrossRef]
31. Song, F.; Bai, L.; Moysiadou, A.; Lee, S.; Hu, C.; Liardet, L.; Hu, X. Transition Metal Oxides as Electrocatalysts for the Oxygen Evolution Reaction in Alkaline Solutions: An Application-Inspired Renaissance. *J. Am. Chem. Soc.* **2018**, *140*, 7748–7759. [CrossRef] [PubMed]
32. Suntivich, J.; May, K.J.; Gasteiger, H.A.; Goodenough, J.B.; Shao-Horn, Y. A Perovskite Oxide Optimized for Oxygen Evolution Catalysis from Molecular Orbital Principles. *Science* **2011**, *334*, 1383–1385. [CrossRef] [PubMed]
33. Zhao, S.; Stocks, A.; Rasimick, B.; More, K.; Xu, H. Highly Active, Durable Dispersed Iridium Nanocatalysts for PEM Water Electrolyzers. *J. Electrochem. Soc.* **2018**, *165*, F82–F89. [CrossRef]
34. Zhang, X.; Liu, F.; Ji, X.; Cui, L.; Li, C.; Liu, J. Facile generation of CeO_2 nanoparticles on multiphased NiS_x nanoplatelet arrays as a free-standing electrode for efficient overall water splitting. *J. Colloid Interface Sci.* **2024**, *653*, 308–315. [CrossRef]
35. Niaz, A.K.; Akhtar, A.; Park, J.-Y.; Lim, H.-T. Effects of the operation mode on the degradation behavior of anion exchange membrane water electrolyzers. *J. Power Sources* **2021**, *481*, 229093. [CrossRef]
36. Chen, Y.; Mojica, F.; Li, G.; Chuang, P.-Y.A. Experimental study and analytical modeling of an alkaline water electrolysis cell. *Int. J. Energy Res.* **2017**, *41*, 2365–2373. [CrossRef]
37. Aykut, Y.; Yurtcan, A.B. Nanostructured electrocatalysts for low-temperature water splitting: A review. *Electrochim. Acta* **2023**, *471*, 143335. [CrossRef]
38. Yuan, S.; Zhao, C.; Cai, X.; An, L.; Shen, S.; Yan, X.; Zhang, J. Bubble evolution and transport in PEM water electrolysis: Mechanism, impact, and management. *Prog. Energy Combust. Sci.* **2023**, *96*, 101075. [CrossRef]

39. Uchino, Y.; Kobayashi, T.; Hasegawa, S.; Nagashima, I.; Sunada, Y.; Manabe, A.; Nishiki, Y.; Mitsushima, S. Relationship Between the Redox Reactions on a Bipolar Plate and Reverse Current after Alkaline Water Electrolysis. *Electrocatalysis* **2018**, *9*, 67–74. [CrossRef]
40. Uchino, Y.; Kobayashi, T.; Hasegawa, S.; Nagashima, I.; Sunada, Y.; Manabe, A.; Nishiki, Y.; Mitsushima, S. Dependence of the Reverse Current on the Surface of Electrode Placed on a Bipolar Plate in an Alkaline Water Electrolyzer. *Electrochemistry* **2018**, *86*, 138–144. [CrossRef]
41. Haleem, A.A.; Huyan, J.; Nagasawa, K.; Kuroda, Y.; Nishiki, Y.; Kato, A.; Nakai, T.; Araki, T.; Mitsushima, S. Effects of operation and shutdown parameters and electrode materials on the reverse current phenomenon in alkaline water analyzers. *J. Power Sources* **2022**, *535*, 231454. [CrossRef]
42. Haleem, A.A.; Nagasawa, K.; Kuroda, Y.; Nishiki, Y.; Zaenal, A.; Mitsushima, S. A New Accelerated Durability Test Protocol for Water Oxidation Electrocatalysts of Renewable Energy Powered Alkaline Water Electrolyzers. *Electrochemistry* **2021**, *89*, 186–191. [CrossRef]
43. Lu, X.; Zhang, Q.; Ng, Y.H.; Zhao, C. Reversible ternary nickel-cobalt-iron catalysts for intermittent water electrolysis. *EcoMat* **2019**, *2*, e12012. [CrossRef]
44. Li, L.; Zhang, G.; Wang, B.; Yang, T.; Yang, S. Electrochemical formation of PtRu bimetallic nanoparticles for highly efficient and pH-universal hydrogen evolution reaction. *J. Mater. Chem. A* **2020**, *8*, 2090–2098. [CrossRef]
45. Hou, Z.-Q.; Liu, R.-W.; Feng, X.-N.; Jia, X.-L.; Huang, K.-J. Durability over 11 days in electrocatalytic hydrogen evolution reaction via designing a 3D magnetic electrode and regulating the electronic structure. *Fuel* **2024**, *357*, 130054. [CrossRef]
46. Babic, U.; Schmidt, T.J.; Gubler, L. Communication—Contribution of Catalyst Layer Proton Transport Resistance to Voltage Loss in Polymer Electrolyte Water Electrolyzers. *J. Electrochem. Soc.* **2018**, *165*, J3016–J3018. [CrossRef]
47. Parache, F.; Schneider, H.; Turpin, C.; Richet, N.; Debellemanière, O.; Bru, É.; Thieu, A.T.; Bertail, C.; Marot, C. Impact of Power Converter Current Ripple on the Degradation of PEM Electrolyzer Performances. *Membranes* **2022**, *12*, 109. [CrossRef] [PubMed]
48. Voronova, A.; Kim, H.; Jang, J.H.; Park, H.; Seo, B. Effect of low voltage limit on degradation mechanism during high-frequency dynamic load in proton exchange membrane water electrolysis. *Int. J. Energy Res.* **2022**, *46*, 11867–11878. [CrossRef]
49. Morrison, A.; Leitch, J.; Szymanski, G.; Moula, G.; Barlow, B.; Burgess, I.; Shobeir, B.; Huang, H.; Lipkowski, J. Mechanism of Electrochemical Dissolution of Nickel Grown by Carbonyl Method. *Electrochim. Acta* **2017**, *248*, 112–122. [CrossRef]
50. Morrison, A.; Leitch, J.; Szymanski, G.; Moula, G.; Barlow, B.; Burgess, I.J.; Shobeir, B.; Huang, H.; Lipkowski, J. Electrochemical dissolution of nickel produced by the Mond method under alternating temperatures and nickel carbonyl gas pressures. *Electrochim. Acta* **2018**, *260*, 684–694. [CrossRef]
51. Iida, M.; Ohtsuka, T. Ellipsometry of passive oxide films on nickel in acidic sulfate solution. *Corros. Sci.* **2007**, *49*, 1408–1419. [CrossRef]
52. Li, A.; Sun, Y.; Yao, T.; Han, H. Earth-abundant transition-metal-based electrocatalysts for water electrolysis to produce renewable hydrogen. *Chem. A Eur. J.* **2018**, *24*, 18334–18355. [CrossRef] [PubMed]
53. Luo, Y.; Zhang, Z.; Yang, F.; Li, J.; Liu, Z.; Ren, W.; Zhang, S.; Liu, B. Stabilized hydroxide-mediated nickel-based electrocatalysts for high-current-density hydrogen evolution in alkaline media. *Energy Environ. Sci.* **2021**, *14*, 4610–4619. [CrossRef]
54. Amireh, S.F.; Heineman, N.N.; Vermeulen, P.; Barros, R.L.G.; Yang, D.; van der Schaaf, J.; de Groot, M.T. Impact of power supply fluctuation and part load operation on the efficiency of alkaline water electrolysis. *J. Power Sources* **2023**, *560*, 232629. [CrossRef]
55. Liu, X.; Pei, Y.; Huang, L.; Lei, W.; Li, F.; Li, Y.; Zhang, H.; Jia, Q.; Zhang, S. Rational design of ultrahigh porosity Co foam supported flower-like FeNiP-LDH electrocatalysts towards hydrogen evolution reaction. *Catal. Today* **2022**, *400–401*, 6–13. [CrossRef]
56. Tang, Y.; Liu, Q.; Dong, L.; Bin Wu, H.; Yu, X.-Y. Activating the hydrogen evolution and overall water splitting performance of NiFe LDH by cation doping and plasma reduction. *Appl. Catal. B Environ.* **2020**, *266*, 118627. [CrossRef]
57. El Haleem, S.M.A.; El Wanees, S.A. Passivation of Nickel in NaOH Solutions. *Prot. Met. Phys. Chem. Surfaces* **2018**, *54*, 859–865. [CrossRef]
58. He, D.; Cao, L.; Huang, J.; Kajiyoshi, K.; Wu, J.; Wang, C.; Liu, Q.; Yang, D.; Feng, L. In-situ optimizing the valence configuration of vanadium sites in NiV-LDH nanosheet arrays for enhanced hydrogen evolution reaction. *J. Energy Chem.* **2020**, *47*, 263–271. [CrossRef]
59. Kulkarni, R.; Lingamdinne, L.P.; Karri, R.R.; Momin, Z.H.; Koduru, J.R.; Chang, Y.-Y. Catalytic efficiency of LDH@carbonaceous hybrid nanocomposites towards water splitting mechanism: Impact of plasma and its significance on HER and OER activity. *Coord. Chem. Rev.* **2023**, *497*, 215460. [CrossRef]
60. Zhang, J.; Zhang, H.; Huang, Y. Electron-rich NiFe layered double hydroxides via interface engineering for boosting electrocatalytic oxygen evolution. *Appl. Catal. B Environ.* **2021**, *297*, 120453. [CrossRef]
61. Zhang, R.; Xu, L.; Wu, Z.; Wang, L.; Zhang, J.; Tang, Y.; Xu, L.; Xie, A.; Chen, Y.; Zhang, H.; et al. Nitrogen doped carbon encapsulated hierarchical NiMoN as highly active and durable HER electrode for repeated ON/OFF water electrolysis. *Chem. Eng. J.* **2022**, *436*, 134931. [CrossRef]
62. Gong, Y.; Wang, L.; Xiong, H.; Shao, M.; Xu, L.; Xie, A.; Zhuang, S.; Tang, Y.; Yang, X.; Chen, Y.; et al. 3D self-supported Ni nanoparticle@N-doped carbon nanotubes anchored on NiMoN pillars for the hydrogen evolution reaction with high activity and anti-oxidation ability. *J. Mater. Chem. A* **2019**, *7*, 13671–13678. [CrossRef]

63. Yonas, S.; Gicha, B.B.; Adhikari, S.; Sabir, F.K.; Tran, V.T.; Nwaji, N.; Gonfa, B.A.; Tufa, L.T. Electric-Field-Assisted Synthesis of Cu/MoS_2 Nanostructures for Efficient Hydrogen Evolution Reaction. *Micromachines* **2024**, *15*, 495. [CrossRef]
64. Tian, Z.; Yang, L.; Wang, Z.; Xu, C.; Li, D. Cost-effective polymetallic selenides derived from stainless steel foam (SSF) for overall water splitting. *Res. Chem. Intermed.* **2021**, *47*, 4779–4787. [CrossRef]
65. Anantharaj, S.; Chatterjee, S.; Swaathini, K.C.; Amarnath, T.S.; Subhashini, E.; Pattanayak, D.K.; Kundu, S. Stainless Steel Scrubber: A Cost Efficient Catalytic Electrode for Full Water Splitting in Alkaline Medium. *ACS Sustain. Chem. Eng.* **2018**, *6*, 2498–2509. [CrossRef]
66. Gao, Y.; Xiong, T.; Li, Y.; Huang, Y.; Li, Y.; Balogun, M.-S.J.T. A Simple and Scalable Approach To Remarkably Boost the Overall Water Splitting Activity of Stainless Steel Electrocatalysts. *ACS Omega* **2019**, *4*, 16130–16138. [CrossRef]
67. Alhakemy, A.Z.; Nassr, A.B.A.A.; Kashyout, A.E.-H.; Wen, Z. Modifying the 316L stainless steel surface by an electrodeposition technique: Towards high-performance electrodes for alkaline water electrolysis. *Sustain. Energy Fuels* **2022**, *6*, 1382–1397. [CrossRef]
68. Yang, R.; Zhou, Y.; Xing, Y.; Li, D.; Jiang, D.; Chen, M.; Shi, W.; Yuan, S. Synergistic coupling of CoFe-LDH arrays with NiFe-LDH nanosheet for highly efficient overall water splitting in alkaline media. *Appl. Catal. B Environ.* **2019**, *253*, 131–139. [CrossRef]
69. Wang, K.; Yu, J.; Liu, Q.; Liu, J.; Chen, R.; Zhu, J. Loading of Single Atoms of Iron, Cobalt, or Nickel to Enhance the Electrocatalytic Hydrogen Evolution Reaction of Two-Dimensional Titanium Carbide. *Int. J. Mol. Sci.* **2024**, *25*, 4034. [CrossRef]
70. Zhang, J.; Deng, W.; Weng, Y.; Jiang, J.; Mao, H.; Zhang, W.; Lu, T.; Long, D.; Jiang, F. Intercalated PtCo Electrocatalyst of Vanadium Metal Oxide Increases Charge Density to Facilitate Hydrogen Evolution. *Molecules* **2024**, *29*, 1518. [CrossRef]
71. Yu, K.; Zhang, J.; Hu, Y.; Wang, L.; Zhang, X.; Zhao, B. Ni Doped Co-MOF-74 Synergized with 2D $Ti_3C_2T_x$ MXene as an Efficient Electrocatalyst for Overall Water-Splitting. *Catalysts* **2024**, *14*, 184. [CrossRef]
72. Gultom, N.S.; Chen, T.-S.; Silitonga, M.Z.; Kuo, D.-H. Overall water splitting realized by overall sputtering thin-film technology for a bifunctional MoNiFe electrode: A green technology for green hydrogen. *Appl. Catal. B Environ.* **2023**, *322*, 122103. [CrossRef]
73. Li, J.; Lin, B.; Zheng, H.; Wang, Y.; Zhang, H.; Zhang, Y.; Nie, Z.; Tang, J. Study on pitting corrosion behavior and semi in-situ pitting corrosion growth model of 304 L SS with elastic stress in NaCl corrosion environment. *Corros. Sci.* **2023**, *211*, 110862. [CrossRef]